

A new experimental setup for making thermal emission measurements in a simulated lunar environment

I. R. Thomas, B. T. Greenhagen, N. E. Bowles, K. L. Donaldson Hanna, J. Temple et al.

Citation: *Rev. Sci. Instrum.* **83**, 124502 (2012); doi: 10.1063/1.4769084

View online: <http://dx.doi.org/10.1063/1.4769084>

View Table of Contents: <http://rsi.aip.org/resource/1/RSINAK/v83/i12>

Published by the [American Institute of Physics](#).

Related Articles

Reflections of ions in electrostatic analyzers: A case study with New Horizons/Solar Wind Around Pluto
Rev. Sci. Instrum. **81**, 114501 (2010)

Wake formation behind positively charged spacecraft in flowing tenuous plasmas
Phys. Plasmas **13**, 062904 (2006)

Propulsion technologies for exploration of the solar system and beyond (plenary)
Rev. Sci. Instrum. **73**, 1079 (2002)

Dustbuster: a compact impact-ionization time-of-flight mass spectrometer for in situ analysis of cosmic dust
Rev. Sci. Instrum. **73**, 185 (2002)

Comparison between simulations and calibrations of a high resolution electrostatic analyzer
Rev. Sci. Instrum. **72**, 3662 (2001)

Additional information on *Rev. Sci. Instrum.*


Journal Homepage: <http://rsi.aip.org>

Journal Information: http://rsi.aip.org/about/about_the_journal


Top downloads: http://rsi.aip.org/features/most_downloaded

Information for Authors: <http://rsi.aip.org/authors>

ADVERTISEMENT



**Does your research require low temperatures? Contact Janis today.
Our engineers will assist you in choosing the best system for your application.**



**10 mK to 800 K
Cryocoolers
Dilution Refrigerator Systems
Micro-manipulated Probe Stations**

**LHe/LN₂ Cryostats
Magnet Systems**

sales@janis.com www.janis.com
Click to view our product web page.

A new experimental setup for making thermal emission measurements in a simulated lunar environment

I. R. Thomas,^{1,a)} B. T. Greenhagen,² N. E. Bowles,¹ K. L. Donaldson Hanna,³ J. Temple,¹ and S. B. Calcutt¹

¹*Atmospheric, Oceanic and Planetary Physics Department, University of Oxford, Oxford, United Kingdom*

²*Jet Propulsion Laboratory, California Institute of Technology, Pasadena, California 91109, USA*

³*Department of Geological Sciences, Brown University, Providence, Rhode Island 02912, USA*

(Received 30 May 2012; accepted 12 November 2012; published online 26 December 2012)

One of the key problems in determining lunar surface composition for thermal-infrared measurements is the lack of comparable laboratory-measured spectra. As the surface is typically composed of fine-grained particulates, the lunar environment induces a thermal gradient within the near sub-surface, altering the emission spectra: this environment must therefore be simulated in the laboratory, considerably increasing the complexity of the measurement. Previous measurements have created this thermal gradient by either heating the cup in which the sample sits or by illuminating the sample using a solar-like source. This is the first setup able to measure in both configurations, allowing direct comparisons to be made between the two. Also, measurements across a wider spectral range and at a much higher spectral resolution can be acquired using this new setup. These are required to support new measurements made by the Diviner Lunar Radiometer, the first multi-spectral thermal-infrared instrument to orbit the Moon. Results from the two different heating methods are presented, with measurements of a fine-grained quartz sample compared to previous similar measurements, plus measurements of a common lunar highland material, anorthite. The results show that quartz gives the same results for both methods of heating, as predicted by previous studies, though the anorthite spectra are different. The new calibration pipeline required to convert the raw data into emissivity spectra is described also. © 2012 American Institute of Physics. [<http://dx.doi.org/10.1063/1.4769084>]

I. INTRODUCTION

A. The Diviner Lunar Radiometer

The primary motivation for this work is the requirement for new thermal-infrared mineral and rock emission spectra to aid in the interpretation of measurements being made by the Diviner Lunar Radiometer.¹ Diviner, launched in June 2009 as part of NASA's Lunar Reconnaissance Orbiter,² is the first lunar orbiting instrument capable of characterizing the shape and location of the Christiansen feature (CF), an infrared spectral feature, with three 8 μm -region channels (7.55–8.05 μm , 8.10–8.40 μm , and 8.38–8.68 μm)¹ allowing new constraints to be placed on thermally derived lunar surface properties.³ By plotting a parabola through the three data points,³ the wavelength of the CF maximum can be mapped across the lunar surface to an accuracy of $\sim 0.03 \mu\text{m}$.⁴

B. Previous measurements

Thermal emission of the lunar surface was first observed using a balloon-borne spectrometer.⁵ In these spectra, the CF was the dominant emission feature observed in the 7–14 μm region measured and shifted in wavelength between locations on the Moon that were believed to be compositionally diverse. When lunar terrestrial analogs^{6–8} and Apollo samples⁹ were measured in the same spectral region in a laboratory, dif-

ferent compositions also exhibited different CF wavelengths. However, the shape and position of this emissivity maximum varied dramatically depending on the conditions under which samples were measured:^{6–8} CFs measured under lunar conditions (Sec. I C) had enhanced spectral contrast with respect to the other spectral features and were, in general, shifted to shorter wavelengths than when measured under ambient conditions (e.g., at atmospheric pressure in room-temperature enclosures).⁷ Further laboratory measurements¹⁰ and thermal models^{11,12} attributed these variations to the creation of a strong temperature gradient due to the solar heating and a reduction in heat transport within the subsurface; the latter of which is caused by the low thermal conductivity of particulate samples and negligible convective heat transport to the very low pressure atmosphere.¹³ On the lunar surface, the penetration depth of the solar diurnal wave (i.e., the depth to which the predominantly visible and near-infrared solar radiation heats the surface) is typically on the order of centimeters. However, the moon re-radiates in the mid-infrared, where the absorption depth is much shorter, allowing only the top layers of the soil to radiate to cold space. These layers are therefore cooled, creating a large (40–50 K per 100 μm depth¹²) thermal gradient within the uppermost $\sim 500 \mu\text{m}$ ¹² of the soil.

When heated isothermally, a sample's spectrum is determined by its spectral emissivity only; however when a thermal gradient is present, variations in transparency affect the measured spectrum. More transparent wavelengths allow radiation from deeper within the surface to radiate out, which are hotter due to the thermal gradient; hence different

^{a)} Author to whom correspondence should be addressed. Electronic mail: thomas@atm.ox.ac.uk.

temperatures are effectively measured at different wavelengths, superimposing the transparency spectrum onto the isothermal emissivity spectrum. The observed wavelength shift in the CF peak is believed to be caused by either: the region of increased transparency being at a slightly shorter wavelength to that of the isothermal emissivity maximum¹² or by a shift in the Planck blackbody radiance peak to shorter wavelengths for higher subsurface temperatures.¹⁴

Spectral measurements made under lunar conditions are very few in number, in contrast to the extensive spectral libraries available for interpretation of Mars' thermal-infrared spectra, for example, and have a limited spectral resolution and range compared to modern spectroscopy laboratories.^{15–17} Logan *et al.*⁸ used a circular variable filter spectrometer (6–11.8 μm range, 1.5% resolution⁶ [i.e., 0.12 μm at 8 μm]) and measured albite, anorthoclase, granite, hornblende, labradorite, olivine, and quartz mineral samples under lunar conditions. Henderson *et al.*¹⁸ measured quartz powder using a grating spectrometer (7–13 μm range, 0.1 μm resolution), though used a different method for generating the thermal gradient (Sec. I C). For interpretation of Diviner data, many more spectra are required, particularly of common lunar minerals such as plagioclases, ortho- and clino-pyroxenes and olivines, plus mixtures, and additional Apollo samples.

C. Replicating the near-surface thermal gradient: Heating the sample cup vs. solar heating

On the lunar, surface heating is provided by the sun, hence the first laboratory experiments heated the samples using a 500 W quartz-iodine lamp, while the samples were held in a low pressure vacuum chamber surrounded by a radiation shield cooled to 77 K.^{6,8,10} Alternatively, the lunar thermal gradient can be replicated by heating samples from below, as demonstrated by Henderson *et al.*,¹⁸ who heated quartz to 500 K while similarly surrounded by a radiation shield held at 100–150 K under a pressure of around 10^{-3} torr ($\sim 10^{-3}$ mbar). These pressures and cold shield temperatures are sufficient to replicate the conditions on the lunar surface: at pressures below $\sim 10^{-3}$ mbar, heat transport by convection is negligible,¹³ and in the mid-infrared, the difference in radiance between a 380 K lunar surface and 150 K shield is equal to the difference between a 380 K surface and 3 K space (e.g., <1% variation at 10 μm). As solar heating penetrates much deeper than the depth from which mid-infrared radiation is emitted,¹² the sun effectively produces heating of the uppermost surface at depth; hence both solar heating and sample cup heating experiments should produce approximately the same thermal gradient. Laboratory experiments¹⁸ showed that for small grain sizes of quartz (0–50 μm , 0–74 μm) the results by heating from below were consistent with solar heating experiments, shifting the CF from 7.35 μm in ambient conditions to around 7.15 μm in lunar conditions, also confirmed in this work (Sec. III). However, minerals other than quartz were not measured by Henderson *et al.*¹⁸ to verify this technique and although the two previous setups both measured the same mineral, each sample had a different grain size distribution, which could have affected the results.

In practice, both types of experimental setup have several advantages and disadvantages. Heating the sample cup is simpler, requiring only high-temperature heater wire and a temperature controller. While this may be useful for measuring pure, fine-grained minerals, it has to be used with caution. For example, measurements of mixtures of different compositions and grain sizes, such as powdered Apollo samples, may have unexpected results. Agglutinates or nano-phase iron particulates¹⁹ could essentially act as an insulating layer, preventing radiation from penetrating samples and altering the thermal gradient. Solar heating experiments are more complex, requiring a solar-like source, and must be designed to prevent reflected light from entering the spectrometer; otherwise the emissivity spectra could be dominated by radiation reflected off the sample. Also, the magnitude of the thermal gradient will be affected by the depth of the sample cup. While the gradient exists in the top few hundred microns, the depth to which sunlight heats the surface is several centimeters and therefore requires a prohibitive amount of sample in many cases. Instead the sample cup needs to be heated to the same temperature as the sample would be at that depth on the lunar surface. Radiative transfer modeling¹¹ has demonstrated that for single-grain sized samples, such temperatures varied from 360 to 460 K depending on the grain size.

To investigate these effects further and to make comparisons between solar and sample cup heating for materials other than quartz, a new setup was required that can replicate the abilities of both. By being able to control both the sample cup temperature and solar light illumination boundary conditions in a single experiment, more detailed investigations can occur, in addition to the measurement of extra sample compositions that have never before been measured under lunar conditions in the laboratory.

II. EXPERIMENTAL SETUP

A. Emission chamber

To make simulated lunar environment (SLE) measurements at higher spectral resolution and across a larger spectral range than previously achieved to support Diviner (and future instrument) data analysis, a new emission spectroscopy chamber was constructed that couples to the emission port of a Brüker IFS-66v/S Fourier transform infrared (FTIR) spectrometer in the Atmospheric, Oceanic and Planetary Physics Department at the University of Oxford, UK.

In this investigation, we constructed new experimental setups (Fig. 1) capable of both sample cup heating and solar source heating (herein referred to as SCH and SSH), consisting of a sample cup surrounded by a radiation shield cooled to <150 K enclosed in a vacuum chamber evacuated to $<10^{-3}$ mbar. The inner surfaces of the radiation shield are painted in Nextel Black high emissivity paint and are cooled by liquid nitrogen flowing through a copper loop attached to the shield. Radiation emitted upwards from the sample is directed into the emission port of the spectrometer by an off-axis parabolic mirror. This mirror fills a significant portion of the sample's field of view and therefore is attached

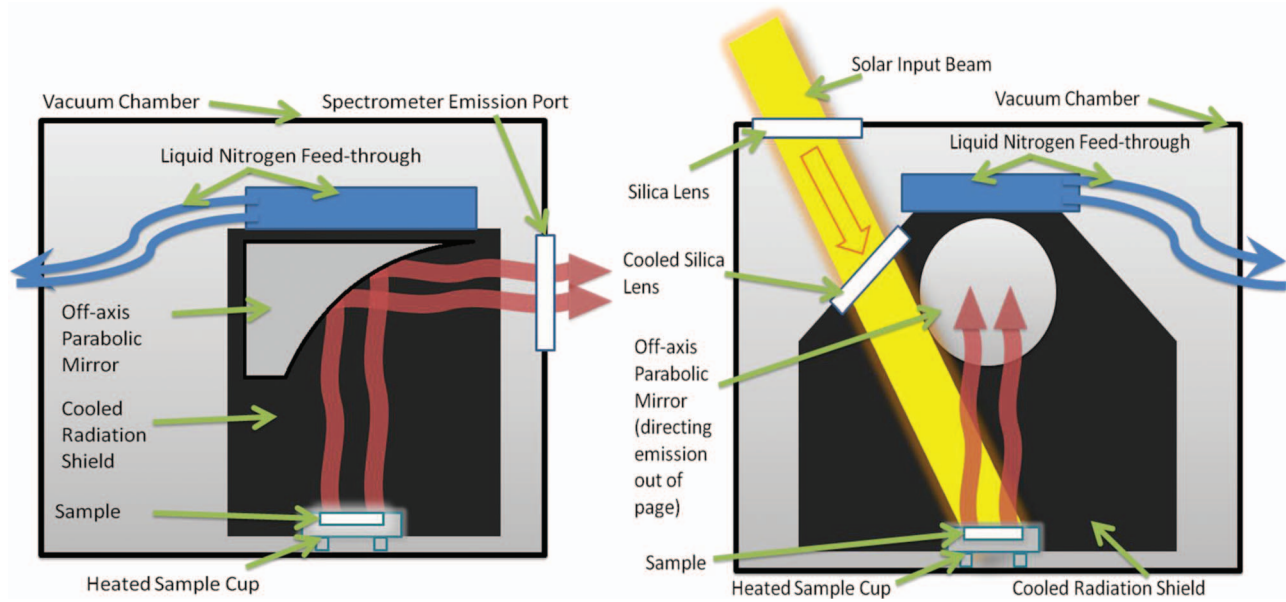


FIG. 1. Diagrams of the lunar environment emission chamber. (Left) The setup required for heating the sample cup only (side view). (Right) The solar heating setup (front view).

to the radiation shield and cooled during SLE experiments. Class B (± 0.3 K at 273 K) platinum resistance thermometers are attached to the sample cup, mirror, and upper and lower radiation shield (to ensure uniform cooling). To prevent water vapor or other contaminants potentially released during sample heating from condensing onto the cooled optics, heater wire is placed within the mirror, keeping the mirror temperature several degrees higher than the shield during the initial cooling stage. In the FTIR spectrometer, a potassium bromide (KBr) emission port window, KBr beamsplitter, and un-cooled DLaTGS detector were used, allowing spectra to be measured typically from 350 cm^{-1} to 3000 cm^{-1} ($3.3\text{ }\mu\text{m}$ to $29\text{ }\mu\text{m}$) at 2 cm^{-1} resolution ($0.01\text{ }\mu\text{m}$ at $8\text{ }\mu\text{m}$).

For solar heating experiments, a 75 W quartz-halogen bulb, similar to that used previously,^{6–8} is shone through two silica windows. The first window removes mid-infrared radiation $>3\text{ }\mu\text{m}$ from the beam to prevent it reflecting off the sample and entering the spectrometer. A second cooled window is required so that as the lamp warms the first window, its infrared emission does not reflect off the sample and subsequently enter the spectrometer.

B. Measurement procedure

Two samples were measured during this study: a 0–30 μm grain size separate of quartz (composition and preparation described elsewhere²⁰) and a 0–25 μm separate of anorthite (composition described elsewhere⁴). Each sample was placed in the emission chamber and initially heated for two hours under vacuum to remove atmospheric contaminants (e.g., water vapor) that could affect the emissivity spectra. First, an ‘ambient’ measurement is made where the sample is heated to 80 °C (353 K) and the radiation shield is held at room temperature, in a chamber of N_2 at atmospheric pressure. The lunar environment can be simulated in two ways:

(1) SCH: the chamber is evacuated to $<10^{-3}$ mbar using a turbo-molecular pump while the sample cup is heated to 500 K and the radiation shield and mirror cooled to <150 K or (2) SSH: the sample cup temperature is set to several values in the range 360–460 K (Sec. I C; Figs. 2 and 3) and the lamp switched on to 75 W, while under a vacuum of $<10^{-3}$ mbar and <150 K radiation shield. For each measurement, 150 scans are co-added using the slowest spectrometer interferometer scan mirror velocity (1.6 kHz). Blackbody spectra are taken at temperatures of 323 K and 348 K consisting of 300 scans each. The raw sample spectra are converted to emissivity as follows.

C. Calibration pipeline

Sample spectra taken under ambient conditions are converted to emissivity using the standard method of FTIR spectrometer emissivity laboratories (described elsewhere^{16,17}) that assumes that the sample is isothermal. For SLE measurements however, a thermal gradient is present in the sample, therefore a new calibration method was developed. This is derived below, starting with the equation by Christensen and Harrison,¹⁵

$$V_{meas}(\lambda, T) = [\varepsilon_{samp}(\lambda)B_{samp}(\lambda, T) + R_{samp}(\lambda)\varepsilon_{env}(\lambda)B_{env}(\lambda, T) - \varepsilon_{inst}(\lambda)B_{inst}(\lambda, T)]F, \quad (1)$$

where $\varepsilon_{samp}B_{samp}$ is the radiance from the sample, $R_{samp}\varepsilon_{env}B_{env}$ is the radiance from the environment reflected off the sample, and $\varepsilon_{inst}B_{inst}$ is the spectrometer radiance. As shown by Ruff *et al.*,¹⁷ two high resolution measurements of a blackbody V_{BB} at two different temperatures T_1 and T_2 are used to calculate the spectrometer response function F and the

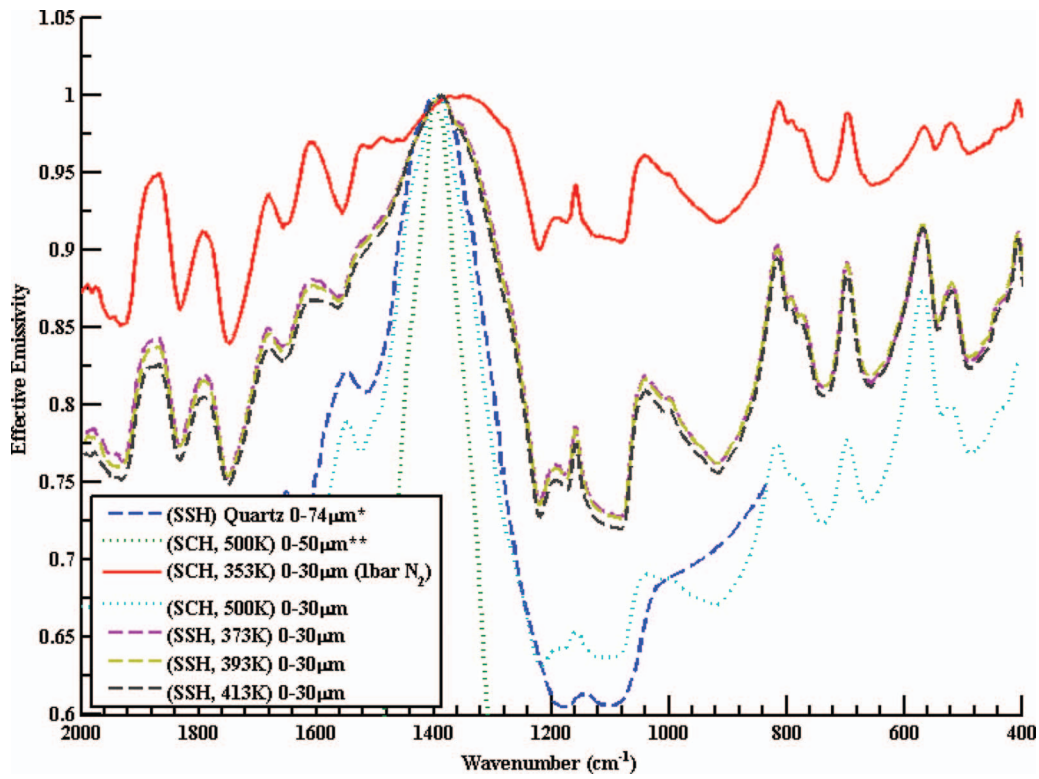


FIG. 2. Comparison of new and previous quartz emissivity spectra, measured under ambient conditions (solid line) or in a SLE by SCH (dotted line) or SSH (dashed line). Sample cup temperature and grain size distribution are given in the legend. (*) Data were digitized from Logan *et al.*⁸ (**) Data were digitized from Henderson *et al.*¹⁸

instrument radiance B_{inst} as follows:

$$F(\lambda) = \frac{V_{BB}(\lambda, T_1) - V_{BB}(\lambda, T_2)}{B_{BB}(\lambda, T_1) - B_{BB}(\lambda, T_2)}, \quad (2)$$

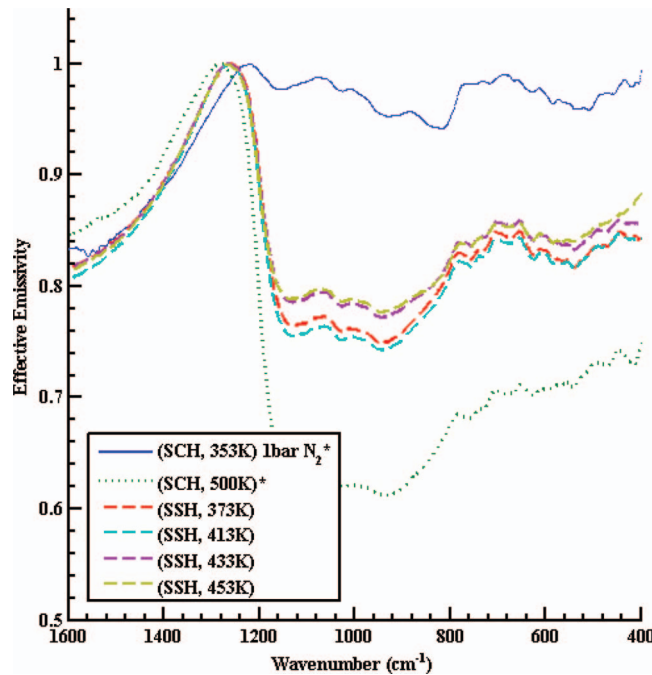


FIG. 3. Emissivity spectra of an anorthite 0-25 μm grain size sample measured in this chamber in ambient conditions (solid line) or in a lunar environment by SCH (dotted) or SSH (dashed), using the sample cup temperature described in the legend. (*) Data taken from Donaldson Hanna *et al.*⁴

$$\varepsilon_{inst}(\lambda)B_{inst}(\lambda, T) = B_{BB}(\lambda, T_2) - \frac{V_{BB}(\lambda, T_2)}{F}, \quad (3)$$

where B_{BB} is the radiance of an ideal blackbody, at temperature T , from the Planck equation. Other emission setups^{16,17} then assume that $R_{samp} = 1 - \varepsilon_{samp}$, but this cannot be assumed here due to the presence of a large thermal gradient within the sample.²¹ Though, with a cooled radiation shield

$$B_{env}(\lambda, T) \ll B_{samp}(\lambda, T), B_{inst}(\lambda, T). \quad (4)$$

Hence, Eq. (1) can be simplified and rearranged to

$$\varepsilon_{samp}(\lambda) = \frac{\varepsilon_{inst}(\lambda)B_{inst}(\lambda, T) + V_{meas}(\lambda, T)/F}{B_{samp}(\lambda, T_{samp})}. \quad (5)$$

Therefore, the sample temperature T_{samp} is calculated so that $\varepsilon_{samp} = 1$ at the peak of the CF.

III. RESULTS

As has been found previously,^{8,18,22} the lunar environment increases the spectral contrast of the CF and shifts the peak to a shorter wavelength, showing the importance of simulating the thermal environment when making measurements in the laboratory (Figs. 2 and 3). The quartz lunar CF wavelengths are all in good agreement, with values of 7.15 μm (Logan *et al.*⁸), 7.1–7.2 μm (Henderson *et al.*¹⁸), 7.12 μm (SCH, this study), and 7.19 μm (SSH, this study); much shorter than the CF measured under ambient conditions at 7.35 μm .⁸ Similarly, the CF position of anorthite shifted from 8.19 μm under ambient conditions to 7.82 μm (SCH) and

7.91 μm (SSH). Error analysis (described in the Appendix) found that the maximum uncertainty in the CF peak wavelength was approximately $\pm 0.03 \mu\text{m}$. An equal uncertainty to this was found when calculating CF peak wavelengths from spectra convolved to Diviner's three 8 μm channels.⁴ While the SCH and SSH derived CF wavelengths for quartz are in some agreement for both minerals, differences in spectral contrast are observed between the two of ~ 0.1 units for the 0–30 μm quartz sample and ~ 0.15 for the anorthite sample. Variations in spectral contrast between the different sized quartz samples (e.g., quartz SSH 0–30 μm in this study and 0–74 μm from Logan *et al.*⁸) are similarly large at ~ 0.15 units of emissivity.

IV. CONCLUSIONS AND FUTURE WORK

- (1) Mineral emissivity spectra taken in a simulated lunar environment differ sufficiently from those taken in ambient conditions; thus determining surface properties, such as composition, using spectral measurements under ambient conditions would lead to incorrect results.
- (2) In the solar heating experiment, using a reasonable sample cup temperature derived from thermal modeling¹¹ produces similar shaped CF, with only a small variation in spectral contrast observed.
- (3) Simulating the lunar environment using the two different methods of heating give similar but not identical results. CF wavelengths are comparable, but variations in spectral contrast are significant, although these are expected due to the non-nadir solar incidence angle (Sec. IC) or differences in particle size between samples (affecting the radiative scattering properties of the sample). It should be noted however that all lunar environmental results are much more similar than to those made in ambient conditions. As such, comparisons should not be made between the spectral contrasts observed in Diviner data and those measured here; however CF wavelengths will correlate.
- (4) In future, emissivity spectra could be extended into the far-infrared using a polyethylene emission port window, Mylar beamsplitter, and far-infrared DLaTGS detector. This would cover most of the range of the Diviner “thermal” channels (13–23 μm , 25–41 μm , 50–100 μm , and 100–400 μm).¹

- (5) This experimental setup is being used⁴ to create a new lunar spectral library. Future studies could use SLE spectra acquired using this setup to investigate regions of the lunar surface observed by Diviner^{3,22} or to test new thermal models.²³

ACKNOWLEDGMENTS

B.T.G. would like to thank J. Hunt at JPL for conducting the Raman spectroscopy of the minerals. I.R.T. would like to thank members of the AOPP electronic and mechanical workshops for their invaluable help and expertise, and the UK Science and Technology Facilities Council for financial support.

APPENDIX: CALCULATION OF THE CHRISTIANSEN FEATURE UNCERTAINTY

For simplicity, all errors were assumed to be uncorrelated and therefore could be added together in quadrature. It was also assumed that the error on calculating the ideal blackbody Planck radiances (B_{BB} , B_{samp} , B_{inst} , etc.) are negligible. The error in spectrometer response function is derived from Eq. (2) as

$$\Delta F(\lambda) = \frac{1}{B_{BB}(\lambda, T_1) - B_{BB}(\lambda, T_2)} \times \sqrt{(\Delta V_{BB}(\lambda, T_1))^2 + (\Delta V_{BB}(\lambda, T_2))^2}, \quad (\text{A1})$$

where the variables are the same as previously described, with a Δ symbol indicating the uncertainty in that variable. The error in spectrometer instrument radiance is calculated from Eq. (3)

$$\begin{aligned} &\Delta(\epsilon_{inst}(\lambda)B_{inst}(\lambda, T)) \\ &= \left(\frac{V_{BB}(\lambda, T_2)}{F} \right) \sqrt{\left(\frac{\Delta V_{BB}(\lambda, T_2)}{V_{BB}(\lambda, T_2)} \right)^2 + \left(\frac{\Delta F}{F} \right)^2}. \end{aligned} \quad (\text{A2})$$

Therefore, the error in emissivity (Fig. 4) is calculated from the error in sample radiance as

$$\begin{aligned} &\Delta(\epsilon_{samp}(\lambda)B_{samp}(\lambda, T_{samp})) \\ &= \sqrt{(\Delta(\epsilon_{inst}(\lambda)B_{inst}(\lambda, T)))^2 + (\Delta(V_{meas}(\lambda, T)/F))^2}, \end{aligned} \quad (\text{A3})$$

$$\Delta\epsilon_{samp}(\lambda) = \sqrt{\left(\left(\frac{V_{BB}(\lambda, T_2)}{F} \right) \sqrt{\left(\frac{\Delta V_{BB}(\lambda, T_2)}{V_{BB}(\lambda, T_2)} \right)^2 + \left(\frac{\Delta F}{F} \right)^2} \right)^2 + \left(\left(\frac{V_{meas}(\lambda, T)}{F} \right) \sqrt{\left(\frac{\Delta V_{meas}(\lambda, T)}{V_{meas}(\lambda, T)} \right)^2 + \left(\frac{\Delta F}{F} \right)^2} \right)^2}. \quad (\text{A4})$$

The uncertainties in $V_{BB}(\lambda, T_1)$, $V_{BB}(\lambda, T_2)$, and $V_{meas}(\lambda, T)$ were determined by running single scans of the quartz 0–30 μm sample and of the blackbody at the two calibration temperatures. The standard deviation $\sigma_{\Delta V}$ was calculated for each

and the standard error was determined from

$$\Delta V(\lambda, T) = \frac{\sigma_{\Delta V}}{\sqrt{n}}, \quad (\text{A5})$$

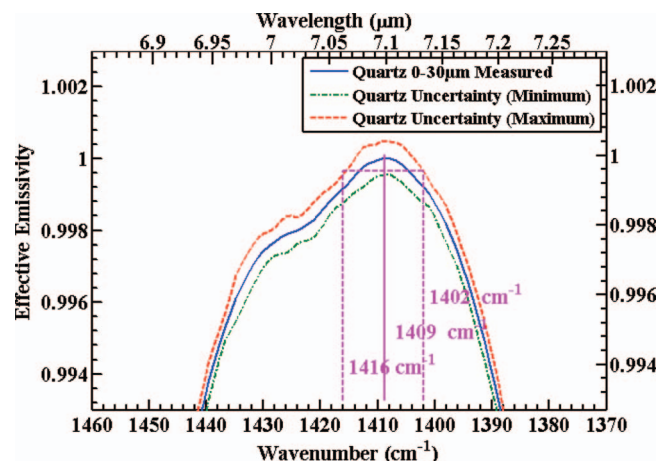


FIG. 4. Calculation of the maximum uncertainty of the quartz 0–30 μm SCH 500 K measurement. In wavelength space, this corresponds to a SCH CF at $7.12 \mu\text{m} \pm 0.03 \mu\text{m}$, smaller than the differences between SCH and SSH. A similar uncertainty will apply to other mineral measurements.

where n is the number of scans taken, i.e., 300 for each black-body and 150 for each sample. More scans can be made to decrease measurement uncertainty further if required, however this would increase the time taken to make the measurements.

¹D. A. Paige, M. C. Foote, B. T. Greenhagen, J. T. Schofield, S. Calcutt, A. R. Vasavada, D. J. Preston, F. W. Taylor, C. C. Allen, K. J. Snook, B. M. Jakosky, B. C. Murray, L. A. Soderblom, B. Jau, S. Loring, J. Bulharowski, N. E. Bowles, I. R. Thomas, M. T. Sullivan, C. Avis, E. M. De Jong, W. Hartford, and D. J. McCleese, *Space Sci. Rev.* **150**(1–4), 125–160 (2010).

²R. Vondrak, J. Keller, G. Chin, and J. Garvin, *Space Sci. Rev.* **150**(1–4), 7–22 (2010).

³B. T. Greenhagen, P. G. Lucey, M. B. Wyatt, T. D. Glotch, C. C. Allen, J. A. Arnold, J. L. Bandfield, N. E. Bowles, K. L. D. Hanna, P. O. Hayne, E. Song, I. R. Thomas, and D. A. Paige, *Science* **329**(5998), 1507–1509 (2010).

⁴K. L. D. Hanna, M. B. Wyatt, I. R. Thomas, N. E. Bowles, B. T. Greenhagen, A. Maturilli, J. Helbert, and D. A. Paige, *J. Geophys. Res., [Planets]* **117**, E00H05, doi:10.1029/2011JE003862 (2012).

⁵F. H. Murcray, D. G. Murcray, and W. J. Williams, *J. Geophys. Res.* **75**(14), 2662–2669, doi:10.1029/JB075i014p02662 (1970).

⁶L. M. Logan and G. R. Hunt, *J. Geophys. Res.* **75**(32), 6539, doi:10.1029/JB075i032p06539 (1970).

⁷L. M. Logan and G. R. Hunt, *Science* **169**(3948), 865 (1970).

⁸L. M. Logan, G. R. Hunt, J. W. Salisbury, and S. R. Balsamo, *J. Geophys. Res.* **78**(23), 4983–5003, doi:10.1029/JB078i023p04983 (1973).

⁹J. W. Salisbury, G. R. Hunt, and L. M. Logan, in *Proceedings of the Lunar Science Conference* (Lunar and Planetary Institute, 1973), Vol. 4, p. 3191.

¹⁰L. M. Logan, G. R. Hunt, and J. W. Salisbury, in *Infrared and Raman Spectroscopy of Lunar and Terrestrial Materials*, edited by J. C. Karr (Academic, New York, 1975), pp. 117–142.

¹¹B. G. Henderson and B. M. Jakosky, *J. Geophys. Res., [Planets]* **99**(E9), 19063–19073, doi:10.1029/94JE01861 (1994).

¹²B. G. Henderson and B. M. Jakosky, *J. Geophys. Res., [Planets]* **102**(E3), 6567–6580, doi:10.1029/96JE03781 (1997).

¹³A. E. Wechsler and P. E. Glaser, *Icarus* **4**(4), 335 (1965).

¹⁴B. Hapke, *J. Geophys. Res., [Planets]* **101**(E7), 16833–16840, doi:10.1029/96JE00918 (1996).

¹⁵P. R. Christensen and S. T. Harrison, *J. Geophys. Res., [Solid Earth]* **98**(B11), 19819–19834, doi:10.1029/93JB00135 (1993).

¹⁶A. Maturilli, J. Helbert, A. Witzke, and L. Moroz, *Planet. Space Sci.* **54**(11), 1057–1064 (2006).

¹⁷S. W. Ruff, P. R. Christensen, P. W. Barbera, and D. L. Anderson, *J. Geophys. Res., [Solid Earth]* **102**(B7), 14899–14913, doi:10.1029/97JB00593 (1997).

¹⁸B. G. Henderson, P. G. Lucey, and B. M. Jakosky, *J. Geophys. Res., [Planets]* **101**(E6), 14969–14975, doi:10.1029/96JE01089 (1996).

¹⁹C. M. Pieters, L. A. Taylor, S. K. Noble, L. P. Keller, B. Hapke, R. V. Morris, C. C. Allen, D. S. McKay, and S. Wentworth, *Meteorit. Planet. Sci.* **35**(5), 1101–1107 (2000).

²⁰B. T. Greenhagen, Ph.D. thesis, University of California, Los Angeles, 2009.

²¹J. W. Salisbury, A. Wald, and D. M. D'Aria, *J. Geophys. Res., [Solid Earth]* **99**(B6), 11897–11911, doi:10.1029/93JB03600 (1994).

²²T. D. Glotch, P. G. Lucey, J. L. Bandfield, B. T. Greenhagen, I. R. Thomas, R. C. Elphic, N. Bowles, M. B. Wyatt, C. C. Allen, K. D. Hanna, and D. A. Paige, *Science* **329**(5998), 1510–1513 (2010).

²³L. Millan, I. Thomas, and N. Bowles, *J. Geophys. Res., [Planets]* **116**, E12003, doi:10.1029/2011JE003874 (2011).